MTL TR 92-19

DEFORMATION AND FAILURE OF 93W-5Ni-2Fe AT HIGH STRAIN RATE SHEAR LOADING

TUSIT WEERASOORIYA, PATRICIA A. BEAULIEU, and
RONALD SWANSON
MATERIALS DYNAMICS BRANCH

April 1992

Approved for public release; distribution unlimited.

US ARMY
LABORATORY COMMAND
MATERIALS TECHNOLOGY LABORATORY

U.S. ARMY MATERIALS TECHNOLOGY LABORATORY
Watertown, Massachusetts 02172-0001

The findings in this report are not to be construed as an official Department of the Army position, unless so designated by other authorized documents.

Mention of any trade names or manufacturers in this report shall not be construed as advertising nor as an official indorsement or approval of such products or companies by the United States Government.

DISPOSITION INSTRUCTIONS

Destroy this report when it is no longer needed.
Do not return it to the originator.

UNCLASSIFIED

SECURITY CLASSIFICATION OF THIS PAGE (When Data Entered)

REPORT DOCUMENTATION PAGE		READ INSTRUCTIONS BEFORE COMPLETING FORM
1. REPORT NUMBER MTL TR 92-19	2. GOVT ACCESSION NO.	3. RECIPIENT'S CATALOG NUMBER
4. TITLE (and Subtitle) DEFORMATION AND FAILURE BEHAVIOR OF 93W-5Ni-2Fe AT HIGH STRAIN RATE SHEAR LOADING		5. TYPE OF REPORT & PERIOD COVERED Final Report
		6. PERFORMING ORG. REPORT NUMBER
7. AUTHOR(s) Tusit Weerasooriya, Patricia A. Beaulieu, and Ronald Swanson		8. CONTRACT OR GRANT NUMBER(s)
9. PERFORMING ORGANIZATION NAME AND ADDRESS U.S. Army Materials Technology Laboratory Watertown, Massachusetts 02172-0001 ATTN: SLCMT-MRD		10. PROGRAM ELEMENT, PROJECT, TASK AREA & WORK UNIT NUMBERS
11. CONTROLLING OFFICE NAME AND ADDRESS U.S. Army Laboratory Command 2800 Powder Mill Road Adelphi, Maryland 20783-1145		12. REPORT DATE April 1992 13. NUMBER OF PAGES 17
14. MONITORING AGENCY NAME & ADDRESS(if different from Controlling Office)		15. SECURITY CLASS. (of this report) Unclassified 15a. DECLASSIFICATION/DOWNGRADING SCHEDULE

16. DISTRIBUTION STATEMENT (of this Report)

Approved for public release; distribution unlimited.

17. DISTRIBUTION STATEMENT (of the abstract entered in Block 20, if different from Report)

18. SUPPLEMENTARY NOTES

19. KEY WORDS (Continue on reverse side if necessary and identify by block number)

Tungsten alloys	Torsion tests
Shear bands	Hopkinson bar
Strain rate	Thermal softening

20. ABSTRACT (Continue on reverse side if necessary and identify by block number)

(See Reverse Side)

DD FORM 1 JAN 73 1473 EDITION OF 1 NOV 65 IS OBSOLETE

UNCLASSIFIED

SECURITY CLASSIFICATION OF THIS PAGE (When Data Entered)

Block No. 20

ABSTRACT

A tungsten heavy alloy containing 93% W (Teledyne 93W-5Ni-2Fe alloy swaged to 17%) was tested in torsion at strain rates of 0.0001, 0.1, and 600 s^{-1} to failure. High rate tests were conducted using a Torsional Split Hopkinson Bar apparatus. The results from these constant strain rate tests show that the yield and failure strengths of this alloy increase with increasing strain rate and the failure strain decreases with increasing strain rate. At 600 s^{-1} strain rate, flow stress decreases with strain, thus indicating thermal softening of the material at high strain rate of deformation. The instability that leads to the initiation of failure at high rate is due to the formation of a localized shear band. The width of the intense shear zone of deformation decreases with increasing shear strain rate reaching a limiting width of one to two grains at high strain rates. As the shear strain rate is increased, there is a reduction in the number of cleavage and brittle grain boundary fracture zones. The results under dynamic conditions show that the 93% W alloy deforms and fails quite differently compared to that under slow rate of loading.

CONTENTS

INTRODUCTION

Tungsten heavy alloys are used in many applications for their mechanical and physical properties such as high density, high strength, good ductility, and good corrosion resistance.[1-3] Tungsten heavy alloys such as 93W-5Ni-2Fe are of interest to the Army as kinetic energy penetrators (replacement for depleted uranium) for defeating armor, because of the high density and excellent mechanical properties. Usually, these mechanical properties are obtained at slow loading rates. Since these alloys are going to be used under dynamic loading conditions by the Army, it is essential to evaluate their mechanical properties and failure behavior under high strain rate loading conditions. Unfortunately, there is very little mechanical property and failure behavior data available for these alloys under dynamic loading conditions.[4-6] Almost all of these available data in the literature have been obtained under uniaxial compressive loading conditions. There are almost no information available under dynamic shear loading conditions. Therefore, this work was undertaken at the U.S. Army Materials Technology Laboratory (MTL) to understand the deformation and failure behavior of a tungsten heavy alloy (WHA) under quasi-static to high shear strain rate loading conditions.

EXPERIMENTS

Material

The 93%W alloy that was used for the experiments in this report was obtained from Teledyne. Chemical composition and some of the mechanical properties of this alloy are:

W	92.85%
Ni	4.9%
Fe	2.25%

Density = 17.69 - 17.76 g/cc

Hardness = HRC 39-40

UTS = 23 MPa (160,000 psi)

Elongation = 13%

---

1. EKBOM, L. M., *Tungsten Heavy Metals*, Scand. J. of Metall., v. 20, 1991, p. 190-197.
2. BOSE, A and GERMAN, R. M., *Sintering Atmosphere Effects on Tensile Properties of Heavy Alloys*, Met. Trans. A, 19A, 1988, p. 2467-2476.
3. DOWDING, R. J., *Tungsten Heavy Alloys: A Tutorial Review*, 1991, P/M in Aerospace and Defence Technologies, MPIF, Princeton, NJ, 1991, p. 109-116.
4. MEYER, L. W. et al., The Proc. of the 7th International Symposium on Ballistics, p. 289-293.
5. THAM, R. and STILP, A. J., *Yield Strength and Flow Stress Measurements of Tungsten Sinter Alloys at Very High Strain Rates*, Journal De Physique, Tome 49, No. 9, C3-85, 1988.
6. ZHANG B. P., ZHENG Y. L., PENG Q. Y. and XIONG Y. M., *Dynamic Behavior of Tungsten Sintered Alloys at High Strain Rates up to 10^5 s^{-1}*, to be published.

This alloy was processed by Teledyne using the following procedure. A mixture of W, Ni, and Fe powder was isostatically pressed to 4.35 MPa (30,000 psi) in a Drybag press. Pressed material was then sintered in a hydrogen atmosphere in a molybdenum furnace at about 1520°C. Hydrogen atmosphere was used to reduce powder surface oxides. The sintered material was vacuum annealed at about 1000°C for 10 hours to remove the absorbed hydrogen. Annealed material was heated in an inert gas atmosphere to about 1100°C and soaked for about an hour. It was then water quenched to give better dynamic impact properties. Then the bars were machined and swaged to 17%.

Figure 1 shows the microstructure of this alloy taken in the longitudinal direction. Microstructure in the transverse direction is similar to the one in the longitudinal direction. Swaging to 17% does not seem to affect the microstructure of the alloy. As shown in the figure, microstructure consists of two phases: nearly pure W spherical grains of bcc crystal structure and W-Ni-Fe matrix of fcc crystal structure. Matrix material provides the ductility for the W alloy with these brittle W grains. The size of W grains are approximately 27 μm and are mostly surrounded by a thin layer of matrix material. However, some of W grains are in contact with the adjacent W grains.

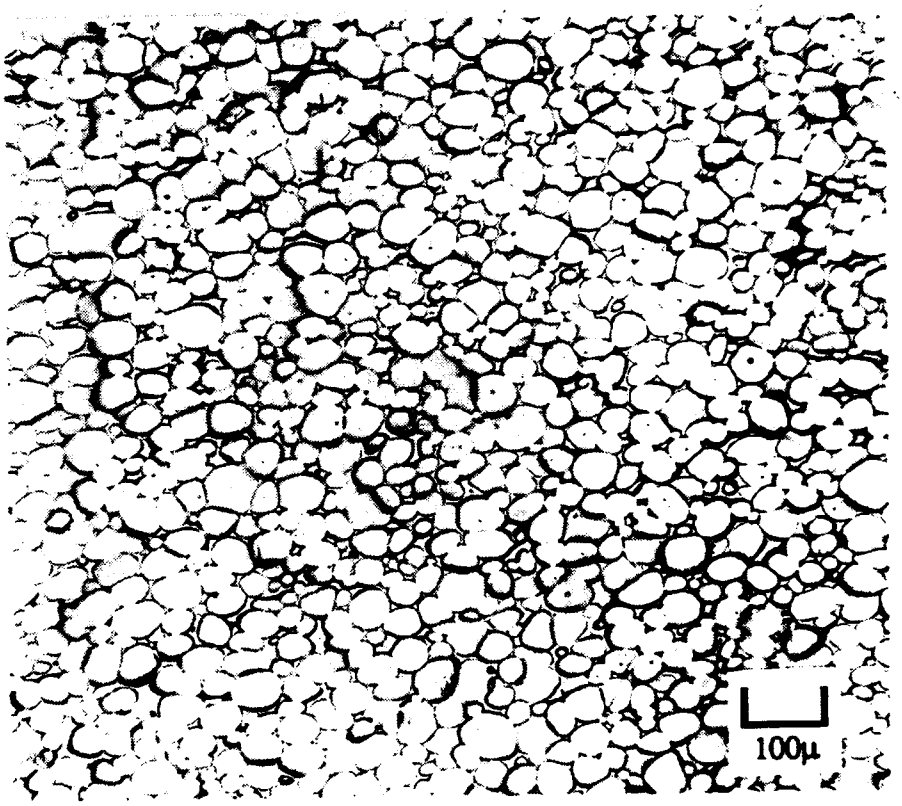

Figure 1. Microstructure of 93W-5Ni-2Fe Tungsten Heavy Alloy swaged to 17%.

Specimen Geometry

Geometry of the test specimen is shown in Figure 2. Gage section of the test specimen is a thin wall tube (0.38-mm wall thickness) of 0.254-mm gage length and outside and inside diameters of 10.16 and 9.40 mm, respectively. The wall thickness corresponds to an average of 14 W grains. Hexagonal flanges with 60° shoulders are machined to both ends of the thin tubular gage section, which are used to attach the specimen to the elastic input and output bars of the test system. Before testing the specimens, parallel to the axis of the specimen a fine line is scribed on the inside wall of the specimen.

In this short gage length specimen, an almost homogeneous state of strain is achieved after a few reflections of the loading shear stress pulse. In a specimen with a similar gage area, but end flanges with sharper (90°) shoulders, the plastic zone starts at the flange-gage section interface. Although the plastic zone starts at this interface, it is contained until it spreads gradually through the specimen and engulfs the whole gage section.[7]

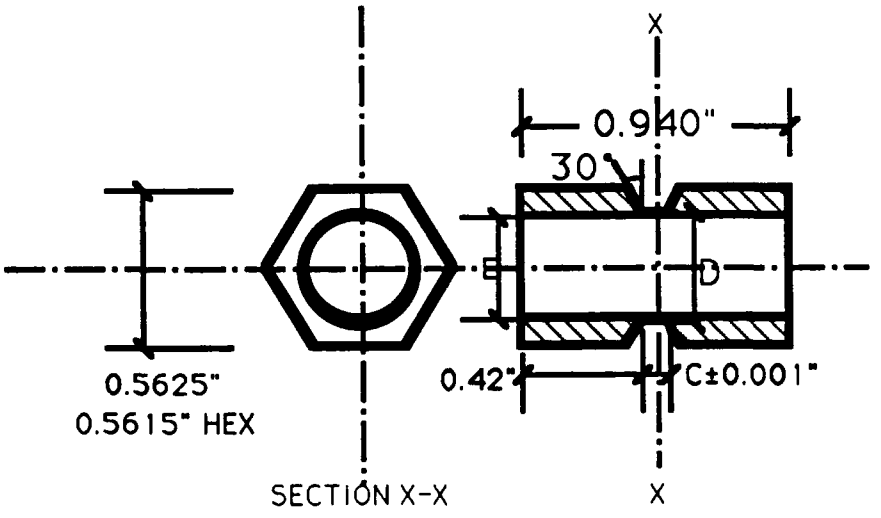

DIM	INCHES	
C	0.100	(0.254 mm)
D	0.400±0.0005 DIA	(10.16 mm)
E	0.370±0.0005 DIA	(9.40 mm)

Figure 2. Specimen geometry.

7. LEUNG, E. K. C., *An Elastic-Plastic Stress Analysis of the Specimen Used in the Torsional Kolsky Bar*. J. Appl. Mech., v. 47, 1980, p. 278.

Torsional Experiments

Thin walled (Teledyne 93% W alloy swaged to 17%) torsion specimens were tested in shear at strain rates of 0.0001, 0.1, and 600 s^{-1} to failure. The high rate (600 s^{-1}) tests were conducted using a Torsional Split Hopkinson Bar apparatus. More details of this apparatus is given by Weerasooriya.[8] Data acquisition and reduction procedure is also described in this report.

A slow rate testing capability was added to this apparatus to achieve strain rates from 0.0001 to 0.1 s^{-1}. A servomotor with a reducer (3600:1) was attached to the end (nonspecimen end) of the output bar. During slow rate testing, the input bar was held stationary using the clamp of the Torsional Split Hopkinson Bar. Linear Variable Differential Transformers (LVDTs) were attached to both input and output bars. Relative rotational displacement between the ends of the gage area was measured using these LVDTs during the slow rate testing. Engineering shear strain of the specimen was calculated using this relative angular displacement. Shear stress was calculated using the thin wall tube assumption for the gage section of the specimen.

After testing, all the specimens were examined with optical and scanning electron microscopes.

RESULTS AND DISCUSSION

Shear stress versus engineering shear strain results for the three different strain rates (0.0001, 0.1, and 600 s^{-1}) are given in Figure 3.

Shear stress - shear strain behavior is strain rate sensitive for this material. Figures 4 and 5 show yield stress and failure strength as a function of logarithmic strain rate, respectively, from the constant strain rate tests. These plots show that both yield and failure strengths increase with strain rate. From the observed linear behavior between the yield stress and the logarithmic value of shear strain rate in Figure 4, following relationship can be obtained relating the shear strain rate ($\dot{\gamma}$) to the yield stress (τ_y):

$$\tau_y = 23 \log_e(\dot{\gamma}) + 732$$

where τ_y is given in MPa and $\dot{\gamma}$ is given in s^{-1}. Total shear strain to failure is plotted as function of logarithmic strain rate in Figure 6. As shown in this figure, total shear strain to failure decreases with increasing strain rate.

For slow strain rates (0.0001 and 0.1 s^{-1}), flow stress increases with increasing shear strain (work hardening). In contrast, at high strain rate of 600 s^{-1}, flow stress decreases with increasing shear strain (softening). This indicates that the thermal softening dominating over work hardening during deformation at high strain rate. The difference in deformation at high strain rate is due to adiabatic heating of the material. Strain to failure at strain rates of 0.0001 and 0.1 s^{-1} are approximately 55% and 48%, respectively. Strain to failure at 600 s^{-1} strain rate is approximately 19%.

---

8. WEERASOORIYA, TUSIT, *The MTL Torsional Split-Hopkinson Bar*, U. S. Army Materials Technology Laboratory, MTL TR 90-27, 1990.

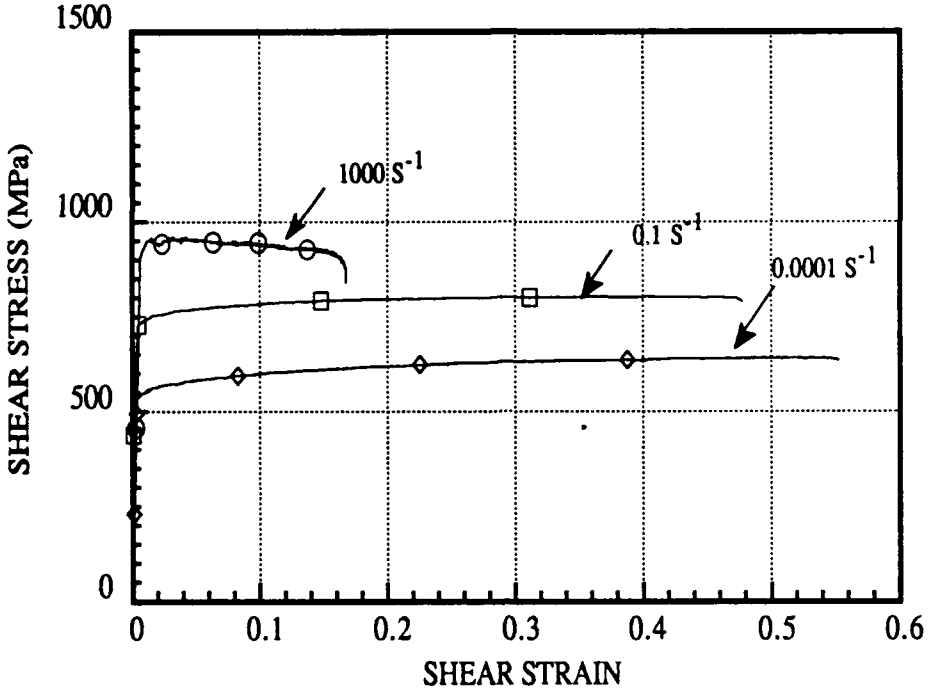

Figure 3. Shear stress - shear strain for 93% W alloy at different strain rates.

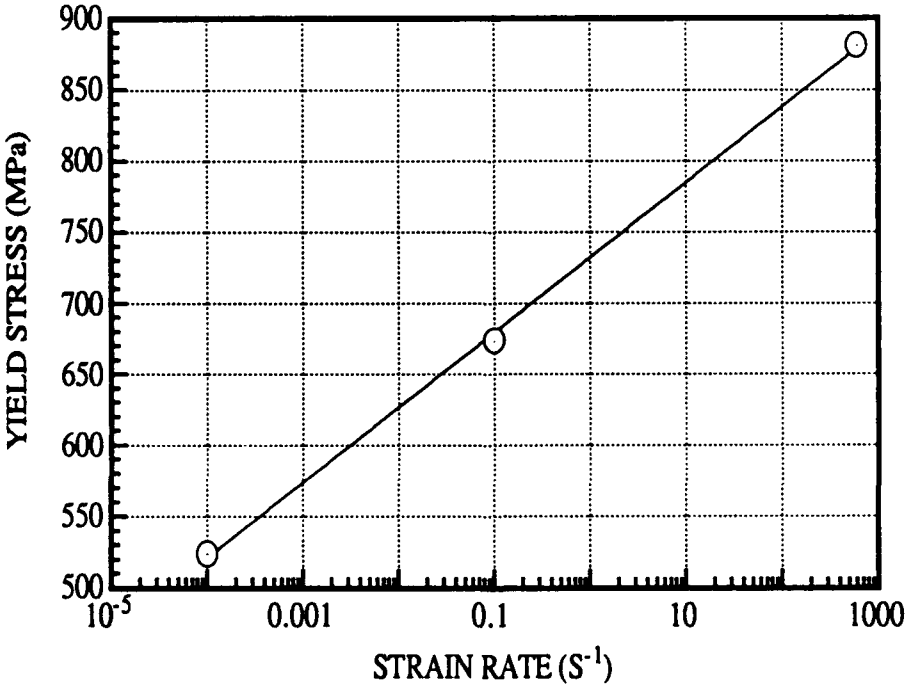

Figure 4. Yield stress as a function of strain rate for 93% W alloy.

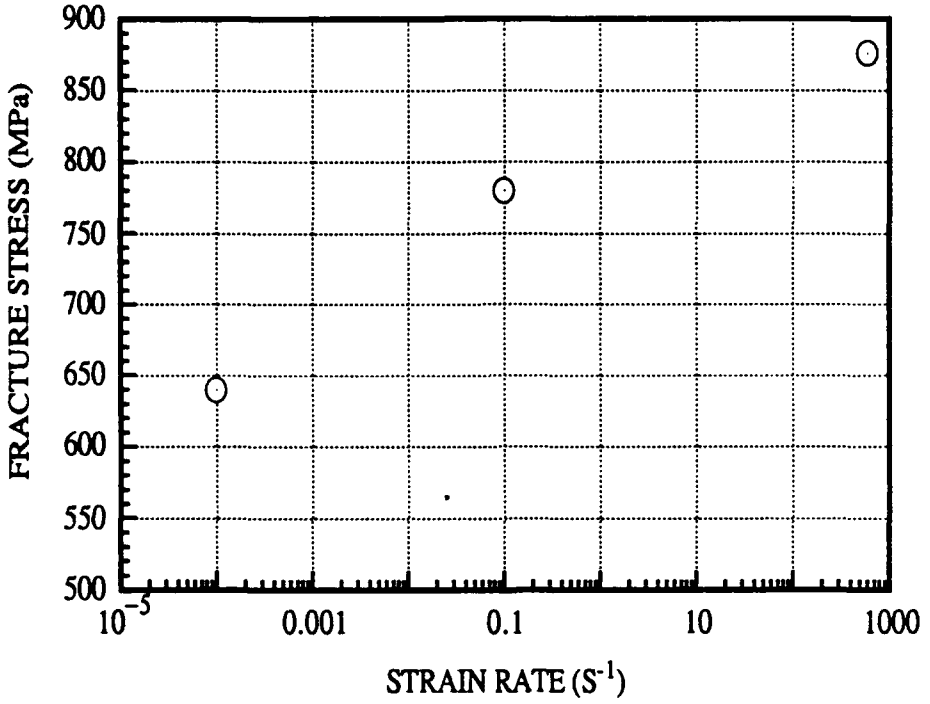

Figure 5. Fracture stress as a function of strain rate for 93% W alloy.

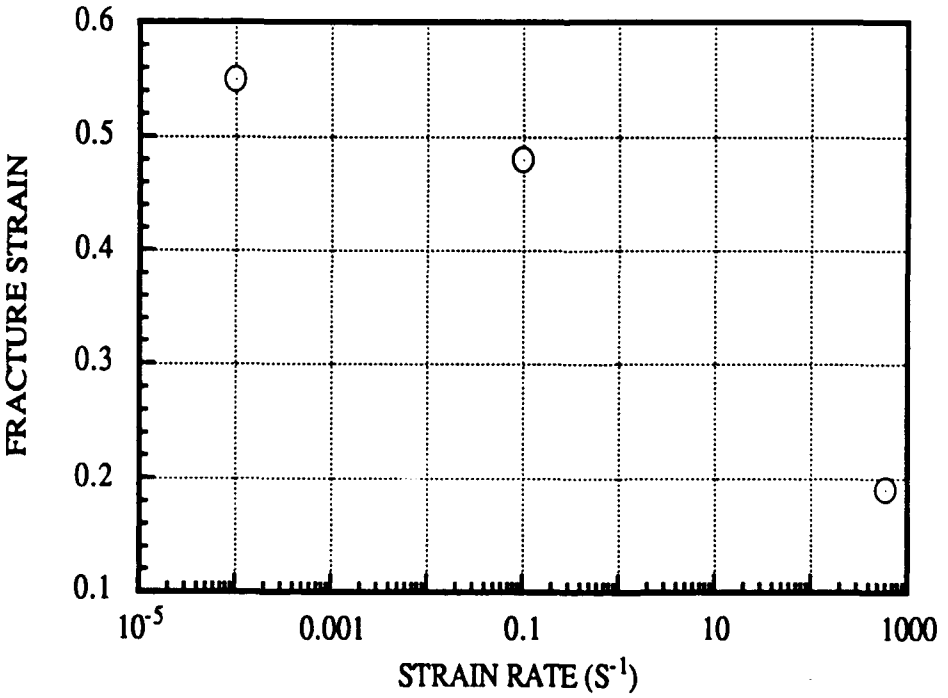

Figure 6. Fracture strain as a function of strain rate for 93% W alloy.

Figures 7 and 8 show the micrographs taken in the vicinity of the fracture surface of the failed specimens at strain rates of 0.0001 and 0.1 s^{-1}, respectively. Closer to the fracture surface, originally spherical W grains have deformed to ellipsoidal shapes. Band of this intense shear zone containing elliptical W grains is approximately 2.14 mm (here the band is defined as two times the width of the zone in the figure) wide for 0.0001 s^{-1} rate and 1.4 mm wide for 0.1 s^{-1}. These ellipses have aligned their major and minor axes 45° to the shear direction. The directions of the major and minor axes correspond to the directions of maximum tensile and minimum compressive principal stresses, respectively. Fracture path is mostly of intergranular, but if a large W grain is blocking the path, fracture will go through the grain splitting the W grain by the cleavage mechanism. This can be seen more clearly in the scanning electron micrographs of the fracture surfaces given in Figure 9. Intergranular and cleavage facets can clearly be observed. Fracture surface from 0.0001 s^{-1} strain rate test shows dimples, typical of ductile fracture, after initial intergranular separation. This indicates that the cavities formed along the grain boundaries coalesce together by the ductile mechanism of fracture of the matrix material separating them. However, the areas showing this typical ductile failure decreases with increasing strain rate.

Figure 10 shows the microstructure at the vicinity of the fracture surface of a failed specimen which was tested at the strain rate of 600 s^{-1}. In this case, in the layer of W grains adjacent to the fracture surface, highly deformed W grains which are of elliptic shape with their major axes aligned 45° to global shear direction can be observed. In contrast to the slower strain rates, here the width of the intense shear zone is much smaller (width of two grains). Figure 11 shows a typical fracture surface of a specimen failed after it has undergone deformation at high rate. Grain boundary facets can be observed as for lower rate tests. Cleavage and ductile dimple-like failure are not present as seen in lower rate tests. Most of the fracture surface is covered with smooth facets. These areas may correspond to W grains that have flowed like a fluid (extruded) during final deformation just before the failure (this process is discussed later in detail). It is not possible to fully explain these areas without any further analysis of this material.

Additional high rate tests were conducted by keeping the width of the shear input pulse constant and gradually reducing the height of the pulse (corresponds to gradually decreasing strain rate). At a strain rate of 400 s^{-1}, it was possible to recover a specimen just before the start of the fracture. Figure 12 gives a micrograph from this specimen showing the initiation of the failure due to the formation of an intense shear band. Width of the shear band is approximately of the size of two to three W grains (100 μm). Length of the shear band is 2.26 mm. Global shear strain at this instant is approximately 20%. Shear strain rate of this test is 400±50 s^{-1}. Since this material is swaged to 17%, an approximate failure point for the annealed material can be assumed to be at a shear strain of 37% (initial prestrain + strain to failure) at this strain rate.

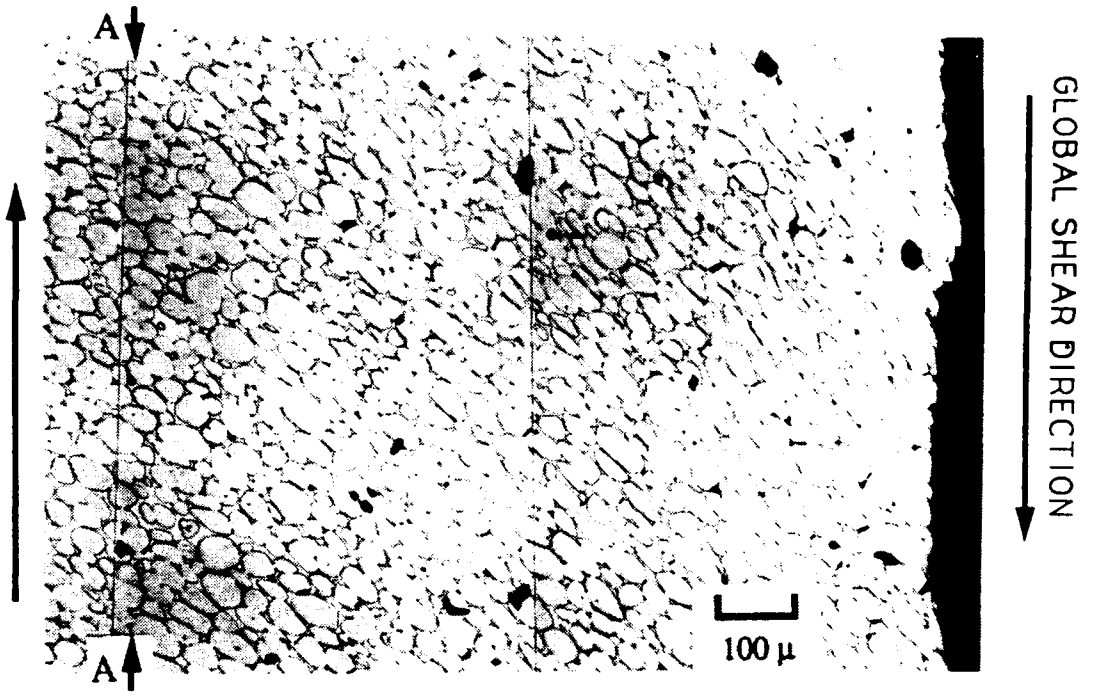

Figure 7. The details of the vicinity of a fractured specimen. Line A-A approximately represents the end of the intensely deformed region. The test was conducted at a shear strain rate of 0.0001 s^{-1} at room temperature. Global shear strain rate at fracture is 55%.

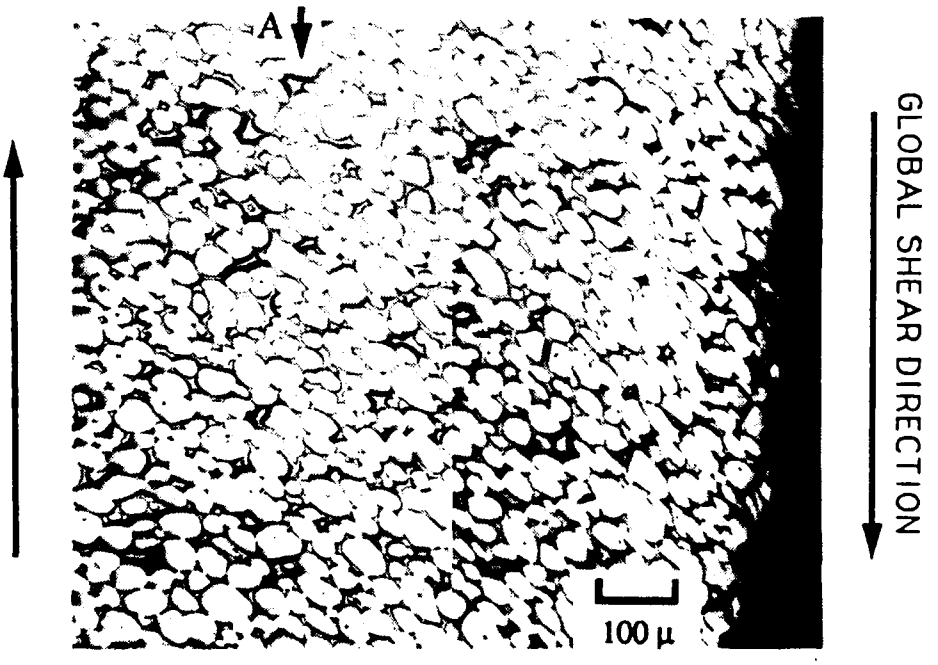

Figure 8. The details of the vicinity of a fractured specimen. Line A-A approximately represents the end of the intensely deformed region. The test was conducted at a shear strain rate of 0.1 s^{-1} at room temperature. Global shear strain rate at fracture is 48%.

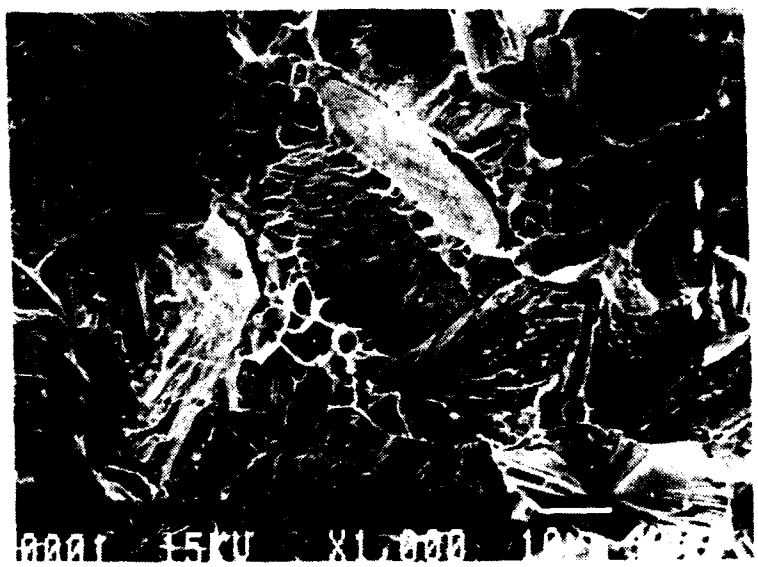

a). Strained at the rate of 0.0001 s^{-1}.

b). Strained at the rate of 0.1 s^{-1}.

Figure 9. Typical fracture surfaces of failed specimens.

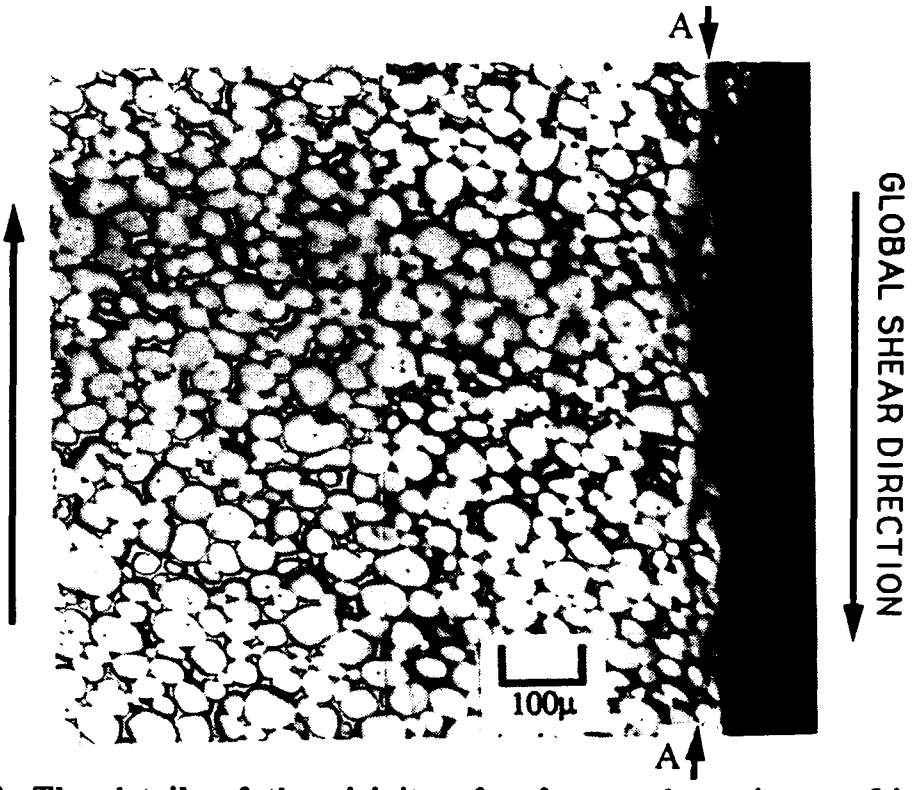

Figure 10. The details of the vicinity of a fractured specimen. Line A-A approximately represents the end of the intensely deformed region. The test was conducted at a shear strain rate of 600 s^{-1} at room temperature. Global shear strain rate at fracture is 19%.

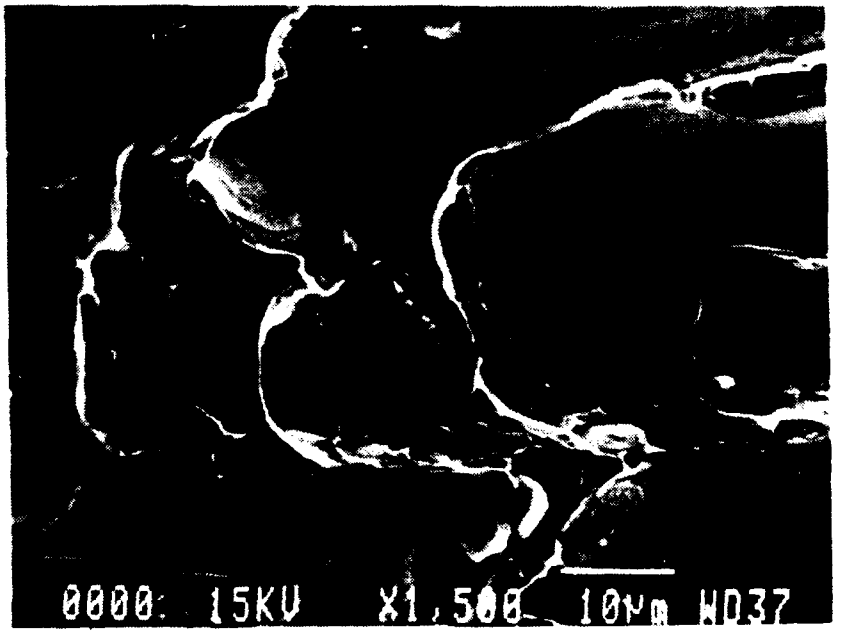

Figure 11. Typical fracture surface of a failed specimen strained at the rate of 600 s^{-1}.

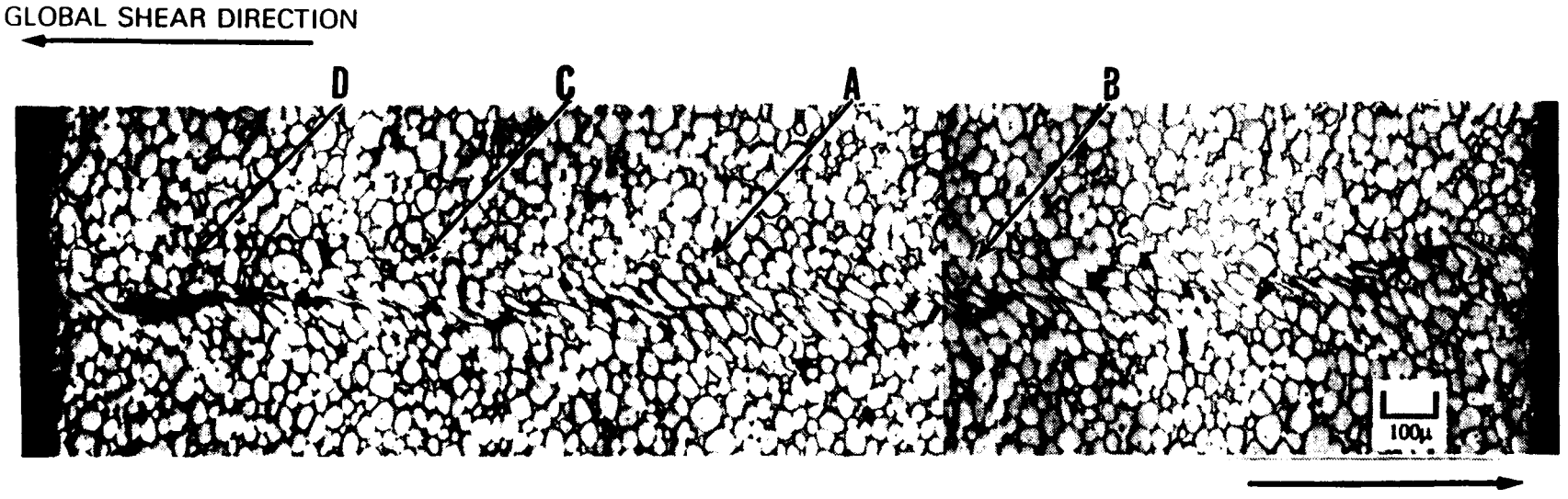

Figure 12. Shear band in 93W-5Ni-2Fe swaged to 17%. The test was conducted at a shear strain rate of 400±50 s^{-1} at room temperature. Global shear strain of the unfractured specimen is 20%. Magnified views of the areas A, B, C and D are given in Figures 13a-d, respectively.

Figures 13a-d show the morphology of various sections of the shear band at double the magnification shown in Figure 12. Different sections of the total shear band show the whole sequence of the formation of the shear band to formation of the final crack which leads to the failure: intense localized deformation of W grains, formation of cavities, coalescence of these cavities to form larger voids and flowing of remaining heavily deformed W grains into these cavities, and the formation of the failure crack. In this intensely deformed shear band, all spherical W grains have deformed to an ellipsoidal form (Figure 13a). Major axis of the ellipse coincides with the maximum tensile principal strain direction and minor axis coincides with minimum compressive principal strain direction. Further tensile straining have opened up cavities at some of these elliptical grains at the locations where the tensile axis meets the grain (see Figure 13b). Some of these cavities initiates at the W-W grain contacts. These cavities have joined to form bigger cavities with the remaining highly deformed W grains flowing into the cavities (Figure 13c). Figure 13c also shows the tear drop like flow of W grains. Figure 13d shows the failure crack formed after joining of these cavities. Additional work is being conducted to characterize sub-structure morphology in the material in the shear band. Results will be reported in a future publication.

SUMMARY AND CONCLUSIONS

Torsional tests were conducted to study the deformation and failure behavior of 93W-5Ni-2Fe alloy at different strain rates. Tests were conducted at three different strain rates: 0.0001, 0.1 and 600 s^{-1}. High rate tests (600 s^{-1}) were conducted using a Torsional Split Hopkinson Bar apparatus. After testing, all the specimens were analyzed using optical and scanning electron microscopes.

From these constant strain rate test results, yield and failure strengths increased with increasing strain rate; failure strain decreased with increasing strain rate. At 600 s^{-1} shear strain rate, flow stress decreased with strain, thus indicating thermal softening of the material at high strain rate. The failure was due to the instability from the formation of a shear band. High strain rates promoted the formation of shear bands. The width of the intense shear zone of deformation decreased with increasing shear strain rate reaching a limiting width of two grains (localized) at high strain rates. As the shear strain rate is increased, there was a reduction in the number of cleavage and brittle grain boundary fracture zones. The results under dynamic conditions showed that the 93% W alloy deformed and failed quite differently compared to that under slow rate of loading. Thus, the materials that are used under dynamic loading conditions should be evaluated under high rate loading conditions.

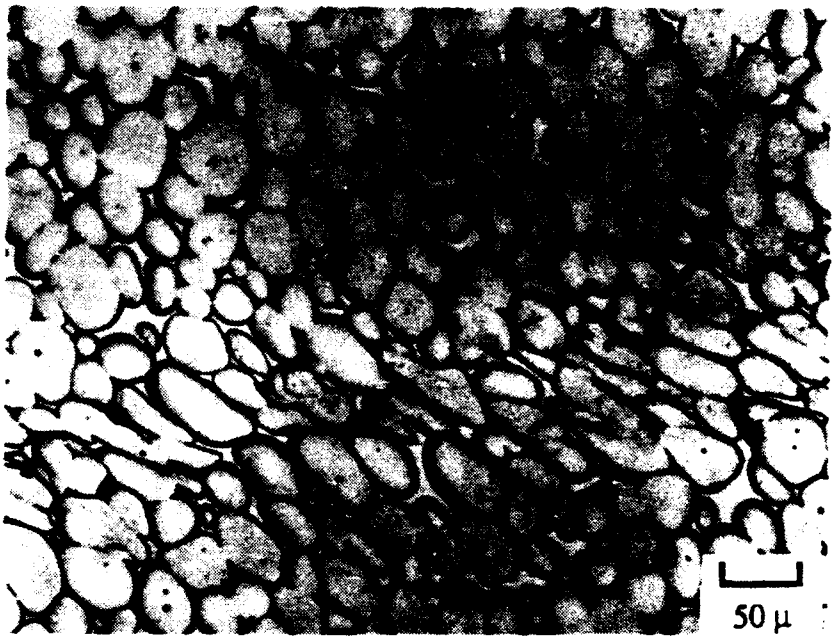

Figure 13a. Intensed localized shear band showing elliptically elongated grains orienting 45° to the global shear direction. This figure corresponds to the area A of the shear band in Figure 12.

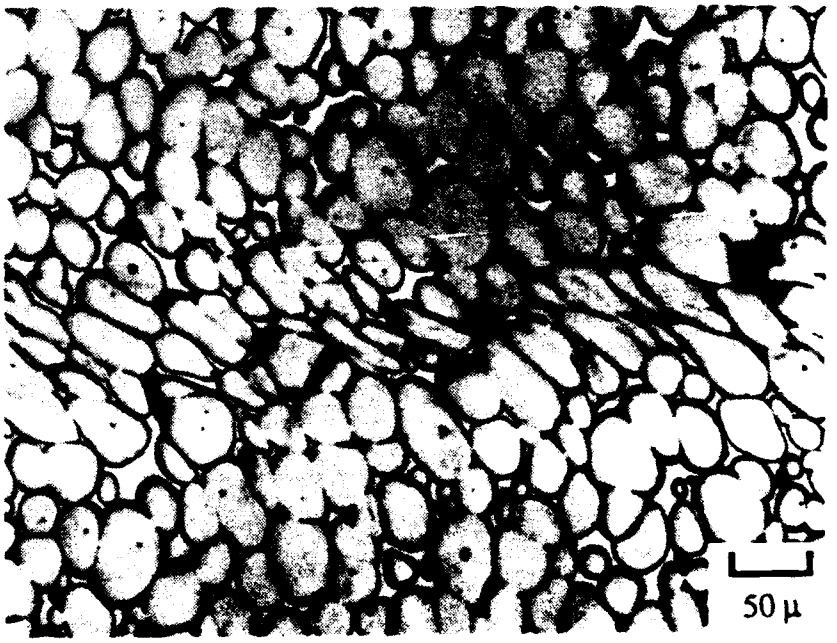

Figure 13b. Formation of cavities at the ends of the major axes of the elliptical grains. This figure corresponds to the area B of the shear band in Figure 12.

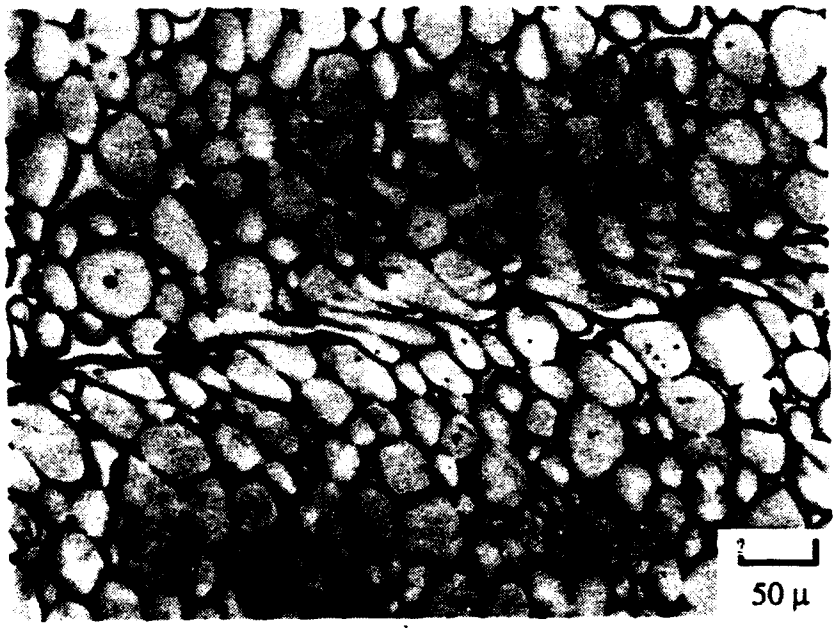

Figure 13c. Coalescence of the cavities forming longer cavities. Elliptical grains have flowed in to these cavities. This figure corresponds to the area C of the shear band in Figure 12.

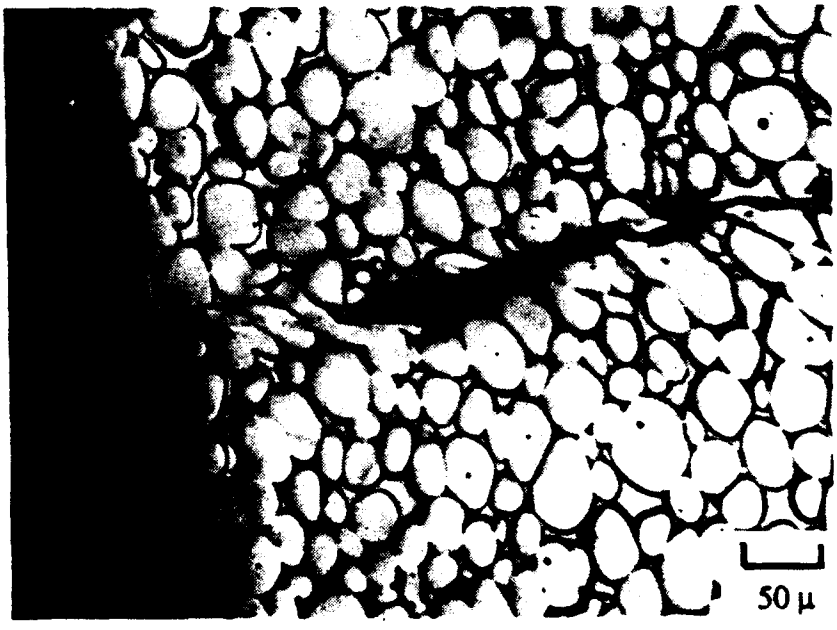

Figure 13d. Formation of the failure crack by the connecting large cavities. Also see the splitting of large W grains in the path of the crack. This figure corresponds to the area C of the shear band in Figure 12.

DISTRIBUTION LIST

No. of Copies	To
1	Office of the Under Secretary of Defense for Research and Engineering, The Pentagon, Washington, DC 20301
	Commander, U.S. Army Materiel Command, 5001 Eisenhower Avenue, Alexandria, VA 22333-0001
1	ATTN: AMCLD
	Commander, U.S. Army Laboratory Command, 2800 Powder Mill Road, Adelphi, MD 20783-1145
1	ATTN: AMSLC-IM-TL
1	AMSLC-CT
	Commander, Defense Technical Information Center, Cameron Station, Building 5, 5010 Duke Street, Alexandria, VA 22304-6145
2	ATTN: DTIC-FDAC
1	MIAC/CINDAS, Purdue University, 2595 Yeager Rd., West Lafayette, IN 47905
	Commander, Army Research Office, P.O. Box 12211, Research Triangle Park, NC 27709-2211
1	ATTN: Information Processing Office
	Commander, U.S. Army Electronics Technology and Devices Laboratory, Fort Monmouth, NJ 07703-5000
1	ATTN: SLCET-DT
	Commander, U.S. Army Missile Command, Redstone Arsenal, AL 35898-5247
1	ATTN: AMSMI-RD-CS-R/Doc
1	Technical Library
	Commander, U.S. Army Armament, Munitions and Chemical Command, Dover, NJ 07801
2	ATTN: SMCAR-TDC
	Commander, U.S. Army Natick Research, Development and Engineering Center, Natick, MA 01760
1	ATTN: Technical Library
	Commander, U.S. Army Tank-Automotive Command, Warren, MI 48397-5000
1	ATTN: AMSTA-R
	U.S. Army ARDEC, Picatinny, NJ 07806
1	ATTN: Bldg 355, Tapan Chattergee
	Commander, U.S. Army Engineer Waterways Experiment Station, P.O. Box 631, Vicksburg, MS 39180
1	ATTN: Research Center Library
	Director, U.S. Army Ballistic Research Laboratory, Aberdeen Proving Ground, MD 21005
1	ATTN: SLCBR-DD-T (STINFO)
1	SLCBR-TB-W, Dr. T. Wright
1	SLCBR-TB-W, Dr. N. J. Huffington
1	SLCBR-TB-W, Dr. J. Walter
	Director, Benet Weapons Laboratory, LCWSL, USA AMCCOM, Watervliet, NY 12189
1	ATTN: AMSMC-LCB-TL
	Commander, U.S. Army Foreign Science and Technology Center, 220 7th Street, N.E., Charlottesville, VA 22901-5396
3	ATTN: AIFRTC, Applied Technologies Branch, Gerald Schlesinger
	Commander, U.S. Army Aviation Systems Command, Aviation Research and Technology Activity, Aviation Applied Technology Directorate, Fort Eustis, VA 23604-5577
1	ATTN: SAVDL-E-MOS
	NASA - Langley Research Center, Hampton, VA 23665
1	ATTN: Aerostructures Directorate
	Naval Research Laboratory, Washington, DC 20375
1	ATTN: Code 5830
	Office of Naval Research, 800 North Quincy Street, Arlington, VA 22217-5000
1	ATTN: Mechanics Division, Code 1132-SM
	Naval Air Development Center, Warminster, PA 18974-5000
1	ATTN: Code 6064
1	AVCSTD/6043

No. of Copies	To
	Naval Surface Warfare Center, Silver Spring, MD 20903-5000
1	ATTN: R. K. Garret, Jr.
	Commander, David Taylor Naval Ship Research & Development Center, Bethesda, MD 20084
1	ATTN: Code 172
	U.S. Air Force Office of Scientific Research, Bolling Air Force Base, Washington, DC 20332
1	ATTN: Mechanics Division
	Commander, U.S. Air Force Wright Research & Development Center, Wright-Patterson Air Force Base, OH 45433-6523
1	ATTN: WRDC/MLLN, Dr. T. Nicholas
	Eglin Air Force Base, FL 32542
1	ATTN: WL/MNMW, Joel House
1	WL/MNMW, W. Cook
	NASA - Marshall Space Flight Center, Huntsville, AL 35812
1	ATTN: EH01, Dir, M&P Lab
1	Prof. Lallit Anand, Massachusetts Institute of Technology, Department of Mechanical Engineering, Cambridge, MA 02139
1	Prof. Robert Asaro, Dept. of Applied Mechanics and Engineering Science, R-011, University of California, San Diego, La Jolla, CA 92093
1	Douglas Baumann, Sandia Laboratories, Div. 8123, P.O. Box 969, Livermore, CA 94305
1	Prof. Romesh Batra, University of Missouri at Rolla, Department of Engineering Mechanics Rolla, MO 65401-0249
1	Dr. Steve Bless, University of Dayton Research Institute, Impact Physics - KLA 14, 300 College Park, Dayton, OH 45469
1	Prof. Stuart Brown, Massachusetts Institute of Technology, Department of Materials Science, Cambridge, MA 02139
1	Dr. Peter C. T. Chen, Benet Weapons Laboratory, B-115, Watervliet, NY 12189-4050
1	Dr. Shin-Chi Chu, ARDEC, ATTN: SMCAR-SCA-TT, Dover, NJ 07801-5001
1	Prof. R. Clifton, Brown University, Division Of Engineering, Providence, RI 02912
1	Prof. J. Duffy, Brown University, Division of Engineering, Providence, RI 02912
1	Dr. S. S. Hecker, Los Alamos National Laboratories, Los Alamos, NM 87545
1	Prof. J. W. Hutchinson, Harvard University, Pierce Hall, Cambridge, MA 02138
1	Gordon R. Johnson, Honeywell Defense Systems Division, 5901 South County Road 18, Edina, MN 55436
1	Prof. Erhardt Krempl, Rensselaer Polytechnic Institute, Department of Mechanical Engineering, Troy, NY 12180-3590
1	Dr. J. Lankford, Southwest Resarch Institute, 6220 Culebra Road, San Antonio, TX 78284
1	Dr. Ulric Lindholm, Southwest Research Institues, P.O. Drawer 28510, San Antonio, TX 78026
1	Prof. Sia Nemat-Nasser, University of California, San Diego, Department of Applied Mechanics and Engineering Sciences, Mail Code B-010, La Jolla, CA 92093
1	Prof. James Rice, Harvard University, Pierce Hall, Cambridge, MA 02138
1	Prof. R. O. Ritchie, University of California, Department of Engineering, Berkely, CA 94720
1	Dr. D. A. Shockey, Stanford Research Institute International, 333 Ravenswood Avenue, Menlo Park, CA 94025
	Laboratoire de Physique, et Mechanique des Materiaux, Faculte' des Sceinces, Ile du Saulcy, 574045, Metz Cedex 1, France
1	ATTN: G. R. Canova
1	J. R. Klepaczko
1	A. Molinari

No. of Copies	To
1	Dr. F. Montheillet, Department Materiaux, Ecole de Mines, 158 Cours Fauriel, 42023 Saint-Etienne, France
	Los Alamos National Laboratories, Materials Science Division, Los Alamos, NM 87545
1	ATTN: G765 Dr. U. F. Kocks
1	G770 Dr. A. D. Rollet
1	G730 Dr. Mike Stout
1	G756 Dr. P. S. Follansbee
1	G730 Dr. T. C. Lowe
	National Institute of Standards, Gaithersburg, MD 20899
1	ATTN: B144 Materials Bldg., Dr. R. J. Fields
	Director, U.S. Army Materials Technology Laboratory, Watertown, MA 02172-0001
2	ATTN: SLCMT-TML
3	Authors

U.S. Army Materials Technology Laboratory,
Watertown, Massachusetts 02172-0001
DEFORMATION AND FAILURE BEHAVIOR OF
93W-5Ni-2Fe AT HIGH STRAIN RATE
SHEAR LOADING -
Tusit Weerasooriya, Patricia A. Beaulieu, and
Ronald Swanson

Technical Report MTL TR 92-19, April 1992, 17 pp-
illustrations

AD ____________

UNCLASSIFIED
UNLIMITED DISTRIBUTION

Key Words

Tungsten alloys
Shear bands
Strain rate

A tungsten heavy alloy containing 93% W (Teledyne 93W-5Ni-2Fe alloy swaged to 17%) was tested in torsion at strain rates of 0.0001, 0.1, and 600 s^{-1} to failure. High rate tests were conducted using a Torsional Split Hopkinson Bar apparatus. The results from these constant strain rate tests show that the yield and failure strengths of this alloy increase with increasing strain rate and the failure strain decreases with increasing strain rate. At 600 s^{-1} strain rate, flow stress decreases with strain, thus indicating thermal softening of the material at high strain rate of deformation. The instability that leads to the initiation of failure at high rate is due to the formation of a localized shear band. The width of the intense shear zone of deformation decreases with increasing shear strain rate reaching a limiting width of one to two grains at high strain rates. As the shear strain rate is increased, there is a reduction in the number of cleavage and brittle grain boundary fracture zones. The results under dynamic conditions show that the 93% W alloy deforms and fails quite differently compared to that under slow rate of loading.

U.S. Army Materials Technology Laboratory,
Watertown, Massachusetts 02172-0001
DEFORMATION AND FAILURE BEHAVIOR OF
93W-5Ni-2Fe AT HIGH STRAIN RATE
SHEAR LOADING -
Tusit Weerasooriya, Patricia A. Beaulieu, and
Ronald Swanson

Technical Report MTL TR 92-19, April 1992, 17 pp-
illustrations

AD ____________

UNCLASSIFIED
UNLIMITED DISTRIBUTION

Key Words

Tungsten alloys
Shear bands
Strain rate

A tungsten heavy alloy containing 93% W (Teledyne 93W-5Ni-2Fe alloy swaged to 17%) was tested in torsion at strain rates of 0.0001, 0.1, and 600 s^{-1} to failure. High rate tests were conducted using a Torsional Split Hopkinson Bar apparatus. The results from these constant strain rate tests show that the yield and failure strengths of this alloy increase with increasing strain rate and the failure strain decreases with increasing strain rate. At 600 s^{-1} strain rate, flow stress decreases with strain, thus indicating thermal softening of the material at high strain rate of deformation. The instability that leads to the initiation of failure at high rate is due to the formation of a localized shear band. The width of the intense shear zone of deformation decreases with increasing shear strain rate reaching a limiting width of one to two grains at high strain rates. As the shear strain rate is increased, there is a reduction in the number of cleavage and brittle grain boundary fracture zones. The results under dynamic conditions show that the 93% W alloy deforms and fails quite differently compared to that under slow rate of loading.

U.S. Army Materials Technology Laboratory,
Watertown, Massachusetts 02172-0001
DEFORMATION AND FAILURE BEHAVIOR OF
93W-5Ni-2Fe AT HIGH STRAIN RATE
SHEAR LOADING -
Tusit Weerasooriya, Patricia A. Beaulieu, and
Ronald Swanson

Technical Report MTL TR 92-19, April 1992, 17 pp-
illustrations

AD ____________

UNCLASSIFIED
UNLIMITED DISTRIBUTION

Key Words

Tungsten alloys
Shear bands
Strain rate

A tungsten heavy alloy containing 93% W (Teledyne 93W-5Ni-2Fe alloy swaged to 17%) was tested in torsion at strain rates of 0.0001, 0.1, and 600 s^{-1} to failure. High rate tests were conducted using a Torsional Split Hopkinson Bar apparatus. The results from these constant strain rate tests show that the yield and failure strengths of this alloy increase with increasing strain rate and the failure strain decreases with increasing strain rate. At 600 s^{-1} strain rate, flow stress decreases with strain, thus indicating thermal softening of the material at high strain rate of deformation. The instability that leads to the initiation of failure at high rate is due to the formation of a localized shear band. The width of the intense shear zone of deformation decreases with increasing shear strain rate reaching a limiting width of one to two grains at high strain rates. As the shear strain rate is increased, there is a reduction in the number of cleavage and brittle grain boundary fracture zones. The results under dynamic conditions show that the 93% W alloy deforms and fails quite differently compared to that under slow rate of loading.

U.S. Army Materials Technology Laboratory,
Watertown, Massachusetts 02172-0001
DEFORMATION AND FAILURE BEHAVIOR OF
93W-5Ni-2Fe AT HIGH STRAIN RATE
SHEAR LOADING -
Tusit Weerasooriya, Patricia A. Beaulieu, and
Ronald Swanson

Technical Report MTL TR 92-19, April 1992, 17 pp-
illustrations

AD ____________

UNCLASSIFIED
UNLIMITED DISTRIBUTION

Key Words

Tungsten alloys
Shear bands
Strain rate

A tungsten heavy alloy containing 93% W (Teledyne 93W-5Ni-2Fe alloy swaged to 17%) was tested in torsion at strain rates of 0.0001, 0.1, and 600 s^{-1} to failure. High rate tests were conducted using a Torsional Split Hopkinson Bar apparatus. The results from these constant strain rate tests show that the yield and failure strengths of this alloy increase with increasing strain rate and the failure strain decreases with increasing strain rate. At 600 s^{-1} strain rate, flow stress decreases with strain, thus indicating thermal softening of the material at high strain rate of deformation. The instability that leads to the initiation of failure at high rate is due to the formation of a localized shear band. The width of the intense shear zone of deformation decreases with increasing shear strain rate reaching a limiting width of one to two grains at high strain rates. As the shear strain rate is increased, there is a reduction in the number of cleavage and brittle grain boundary fracture zones. The results under dynamic conditions show that the 93% W alloy deforms and fails quite differently compared to that under slow rate of loading.